Journal of Magnetic Resonance **136,** 200–206 (1999)
Article ID jmre.1998.1657, available online at http://www.idealibrary.com on IDEAL®

A New Q-Band EPR Probe for Quantitative Studies of Even Electron Metalloproteins

D. T. Petasis and M. P. Hendrich

Department of Chemistry, Carnegie Mellon University, Pittsburgh, Pennsylvania 15213

Received August 7, 1998; revised November 6, 1998

Existing Q-band (35 GHz) EPR spectrometers employ cylindrical cavities for more intense microwave magnetic fields B_1, but are so constructed that only one orientation between the external field B and B_1 is allowed, namely the $B \perp B_1$ orientation, thus limiting the use of the spectrometer to measurements on Kramers spin systems (odd electron systems). We have designed and built a Q-band microwave probe to detect EPR signals in even electron systems, which operates in the range $2\ K \leq T \leq 300\ K$ for studies of metalloprotein samples. The cylindrical microwave cavity operates in the TE_{011} mode with cylindrical wall coupling to the waveguide, thus allowing all orientations of the external magnetic field B relative to the microwave field B_1. Such orientations allow observation of EPR transitions in non-Kramers ions (even electron) which are either forbidden or significantly weaker for $B \perp B_1$. Rotation of the external magnetic field also permits easy differentiation between spin systems from even and odd electron oxidation states. The cavity consists of a metallic helix and thin metallic end walls mounted on epoxy supports, which allows efficient penetration of the modulation field. The first quantitative EPR measurements from a metalloprotein (Hemerythrin) at 35 GHz with $B_1 \parallel B$ are presented. © 1999 Academic Press

INTRODUCTION

The active centers of many metalloproteins contain metal ions with an odd number of electrons and thus have a half-integer electronic spin ($S = 1/2, 3/2, \ldots$). These so-called Kramers ions have zero-field spin manifolds, where the states exhibit at least a two-fold degeneracy, and are thus amenable to study by conventional EPR spectroscopy. Such spin states split linearly in an applied magnetic field **B** (Fig. 1(a)) and spin transitions can be induced provided the resonance condition $h\nu = g_{\text{eff}}\beta B$ is satisfied, with the selection rule $\Delta m_s = \pm 1$. Due to the relative simplicity of the spectroscopy of these ions, most EPR instrumentation was developed with the aim of studying such ions. However, many metalloproteins contain metal ions with an even number of electrons and consequently an integral electronic spin ($S = 1, 2, \ldots$) or contain ion pairs which interact to give a total even electron system and a total integer-spin (*1, 2*). A pair of energy levels of these spin systems have zero-field splitting Δ, and a quadratic energy splitting as a function of an applied field **B** (Fig. 1(b)). The resonance condition for these levels is consequently more complex than in the case of Kramers ions and is given by (*3*)

$$(h\nu)^2 = (g_{\text{eff}}\beta B)^2 + \Delta^2. \qquad [1]$$

The spin states for such non-Kramers doublets are symmetric and antisymmetric combinations of $|m_s\rangle$, $|\pm m_s'\rangle = |+m_s\rangle \pm |-m_s\rangle$, thus m_s is no longer a good quantum number. Historically, the selection rule for such doublets has been written as $\Delta m_s = \pm 2, \pm 4, \ldots$; however, the transition matrix element giving signal intensity is $\langle +m_s'|S_z|-m_s'\rangle \neq 0$, thus we prefer the selection rule $\Delta m = 0$ (*1*).

The rationale for the construction of a new cavity is a consequence of the preceding two fundamental differences between odd and even electron ions, namely, the resonance condition and selection rule. For even electron ions with $\Delta > h\nu$, the doublet energy splitting exceeds the microwave quantum, Eq. [1] cannot be satisfied, and no resonance is observed. Thus, the observation of EPR signals requires higher frequency spectrometers for which $h\nu > \Delta$. The different selection rules affect the intensity of signals. EPR signal intensities are strongly dependent on the orientation of the microwave magnetic field $\mathbf{B_1}$ relative to the static field **B**. The intensity of transitions for isolated doublets of odd electron ions is $I \sim |\langle +m_s|\mathbf{B_1}\cdot\mathbf{S}|-m_s\rangle|^2 = |\langle +m_s|B_{1x}S_x + B_{1y}S_y|-m_s\rangle|^2$. Since the quantization axis, *z*, is always parallel to **B**, only components of $\mathbf{B_1} \perp \mathbf{B}$ contribute to the signal intensity. In contrast, the signal intensity from a doublet of even electron ions is $I \sim |\langle +m_s'|\mathbf{B_1}\cdot\mathbf{S}|-m_s'\rangle|^2 = |\langle +m_s'|B_{1z}S_z|-m_s'\rangle|^2$, and thus, only components of $\mathbf{B_1}$ parallel to the *z* axis contribute to the signal intensity. Also, for even ion systems, the direction of the quantization *z* axis is determined by the molecule rather than **B**; consequently, signal intensities are strongly dependent on molecular orientation. Signal intensities are typically significantly larger with $\mathbf{B_1} \parallel \mathbf{B}$ than $\mathbf{B_1} \perp \mathbf{B}$ for powder samples, because the resonance field becomes exceedingly large for $\mathbf{B} \perp z$.

To facilitate observation of EPR signals from metalloproteins with even electron systems, the new instrumentation development takes into consideration these differences in the

1090-7807/99 $30.00

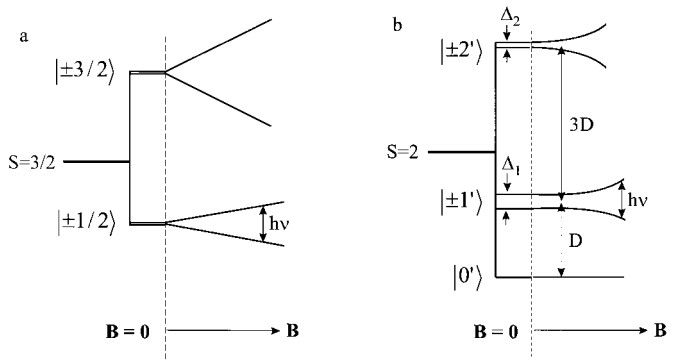

FIG. 1. Comparison of energy level diagrams of (a) Kramers ($S = 3/2$), and (b) non-Kramers ($S = 2$) ions. For $S = 2$: $\Delta_1 = 6E$ and $\Delta_2 = 3E^2/D$, where D and E are defined by Eq. [2].

resonance condition and selection rule. First, it is apparent from the preceding discussion and previous work that the ability to change the orientation of $\mathbf{B_1}$ is of great utility, since paramagnetic oxidation states which differ by a single electron are then readily distinguishable. For $\mathbf{B_1} \parallel \mathbf{B}$, signals from even electron ions have maximal intensity, whereas signals from odd-electron ions vanish. In response to demand for such applications, Bruker Instruments now manufactures a microwave cavity operating near 9 GHz, which is similar to that first commercially available from Varian. Second, the resonance condition given by Eq. [1] contains two unknowns, g_{eff} and Δ, thus a second microwave frequency is required to determine both unknowns. This second frequency should be greater than 9 GHz (X-band) to facilitate observation of signals from proteins with $\Delta > h\nu = 0.3\ \text{cm}^{-1}$.

One such spectrometer capable of orienting $\mathbf{B_1} \parallel \mathbf{B}$, operating at 95 GHz, has been reported by Disselhorst *et al.* (*4*). This pulsed EPR spectrometer has considerable potential for metalloprotein studies as has been demonstrated in a study of the copper protein azurin (*5*). The capability of measurements at 95 GHz on the typically much broader resonance from even electron metalloproteins remains to be seen, but a pulsed system may be especially suited since magnetic field modulation is not a limiting factor. A number of other spectrometers at 95 GHz and higher frequencies have been used in studies of inorganic metals (*6*). At these frequencies interdoublet transitions for $S > 1/2$ spin systems become possible, however, none of these spectrometers have yet been shown to be sufficiently sensitive for studies of metalloproteins. Our goal was the design of a probe at a microwave frequency significantly higher than X-band which would most likely have sufficient sensitivity for studies of metalloprotein samples. Typically such samples are limited to concentrations of less than several millimolar. In addition, we decided to choose a microwave frequency for which a commercial bridge and console was available. Thus, we have combined the existing technologies in spectrometers, microwave cavities, and immersion cryogenic systems to create a new configuration especially suited for metalloprotein studies.

These concerns have prompted us to design and build a Q-band ($\nu \sim 34$ GHz, $1/\lambda \approx 1.2\ \text{cm}^{-1}$) microwave probe capable of quantitative measurements on even electron metal centers. Commercial and various "home-built" EPR spectrometers operating at Q-band all employ the conventional end-wall microwave coupling to the cavity, and thus only allow $\mathbf{B_1} \perp \mathbf{B}$ (*7*, *8*). Our spectrometer employs a cylindrical cavity coupled to the EPR probe through the cylindrical surface instead of the conventional coupling through the end wall (*9*), thus allowing $\mathbf{B}$ to be oriented both parallel or perpendicular (or any intermediate angle) to $\mathbf{B_1}$ (Fig. 2). A cavity coupled through the cylindrical wall of the cavity presents many engineering difficulties: (1) inherently lower Q, (2) poor penetration of $\mathbf{B}_{\text{mod}}$ through the end walls for the parallel mode, (3) noise from vibrating end walls due to eddy current loops in parallel mode necessitating special locking devices, (4) a locked plunger making tunability at low temperatures impossible, and (5) the inability to load sample while the cavity is immersed in the cryostat. However, the cylindrical wall coupling design has the overwhelming advantage of allowing reorientation of $\mathbf{B}$ with respect to $\mathbf{B_1}$ with a rotatable magnet, whereas the conventional coupling design only allows $\mathbf{B}$ to rotate in a plane which is always perpendicular to $\mathbf{B_1}$. Other cylindrical cavity modes, such as TM_{011}, allow end-wall coupling and orientations where $\mathbf{B_1} \parallel \mathbf{B}$ but have other drawbacks, the most significant of which is the lack of tunability to the narrow range of most available microwave sources. A right-angle bend of the microwaves prior to a conventional end-wall cavity entrance was also deemed not practical, due to eddy current generation in the microwave guide and the problems of liquid helium heating and low modulation penetration. While it is advantageous to lower the modulation frequency to reduce such eddy currents, the spectrometer sensitivity is often dominated by the intensity of the magnetic field modulation at the sample. Less metal, e.g., no microwave guide right angle at a cavity wall, allows additional modulation intensity at any given frequency prior to eddy current noise generation.

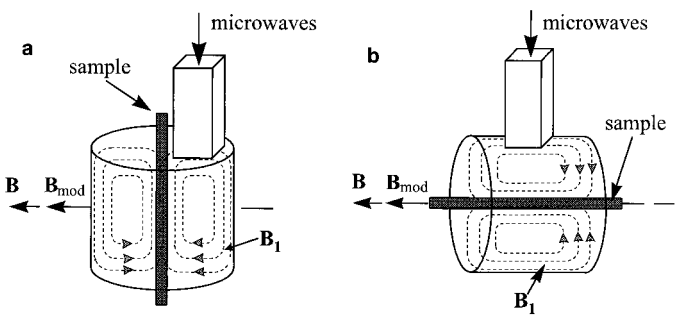

FIG. 2. Comparison of coupling methods: (a) conventional end-wall coupling and (b) cylindrical-wall coupling. $\mathbf{B}$ = applied magnetic field, $\mathbf{B}_{\text{mod}}$ = modulation field, $\mathbf{B_1}$ = magnetic field component of microwave radiation. In (b), $\mathbf{B}$ rotates in a plane at right angles to the page.

As demonstrated here, we have overcome the engineering difficulties in the cylindrical wall coupling to produce a probe and cryogenic system capable of measurements on even or odd electron metalloproteins. These are the first data above X-band microwave frequencies to produce spectra from a parallel mode configuration on an even electron metalloprotein. In addition, the ability to quantitatively analyze the spectra to determine metal center concentration is demonstrated with the use of accurate simulations of the spectra. This is an essential utility needed to address the common problem of assessing whether signals originate from impurities or biologically relevant species.

PROBE CONSTRUCTION

Cylindrical Cavity

A cylindrical cavity, rather than a rectangular cavity, is preferred at these frequencies since it has a higher microwave energy density and can be tuned easily (*9–11*). The TE_{011} cylindrical mode is the mode of choice because it has a maximum microwave magnetic field along the axis of symmetry of the cavity, which is a suitable location for the sample. The cavity is of helical construction, which allows transparent penetration of the modulation field both parallel and perpendicular to the cavity axis.

Our helical cavity was constructed from a brass or pure silver mandrel having a length of 1.00 in. and diameter of 0.528 in., with 12 threads/in. (American National Thread) cut on the outside of the body. The threads have a depth of 0.033 in. and a separation of 0.010 in. The mandrel is cast in epoxy using a method similar to that described by Wang and Chasteen (*8*). The dimensions of the cavity are dictated by the guide wavelength (λ_g = 0.462 in.) and the maximum Q condition, which requires the length of the cavity (d) to be equal to its diameter (2a) (*9*). The mandrel is bored out to form the cavity with a diameter of 0.462 in. and a length of 0.520 in., which can be adjusted by a movable plunger (Fig. 3). The depth of the brass thread left inside the epoxy is 0.030 in. with a thickness of 0.065 in. and a thread separation of approximately 0.010 in. The edge to edge distance between the threads of the helix is 0.140 in. allowing a coupling hole of 0.130 in. to be drilled between two adjacent threads and still maintain critical electrical continuity of the helix. The coupling hole is placed at a distance of $\lambda_g/4$ from the end wall for optimum coupling (*12*). The microwaves are coupled from the waveguide into the cavity with the Gordon coupler shown in Fig. 3. The cavity proved to be very robust and withstood a large number of temperature cyclings.

Frequency tuning of the cavity is achieved by a movable end wall (plunger). A plunger with a nonmetallic barrel minimizes the amount of metal seen by the modulation field when parallel to the cavity axis. To construct the plunger, a thin brass disc (0.420 in. diameter, 0.010 in. thickness) with a 0.030 in. thick lip on its rim, to anchor the wall in the epoxy, was placed at the bottom of a Teflon split-mold which was filled with epoxy and cured. The plunger was threaded (20 threads/in., Acme thread), and the face of the plunger was carefully machined down to a final thickness of 0.002–0.003 in. for maximum modulation penetration. The stationary wall is solid brass with thickness 0.002–0.003 in., molded with epoxy. With these walls, we find 70–75% of the expected modulation at 100 kHz in the sample

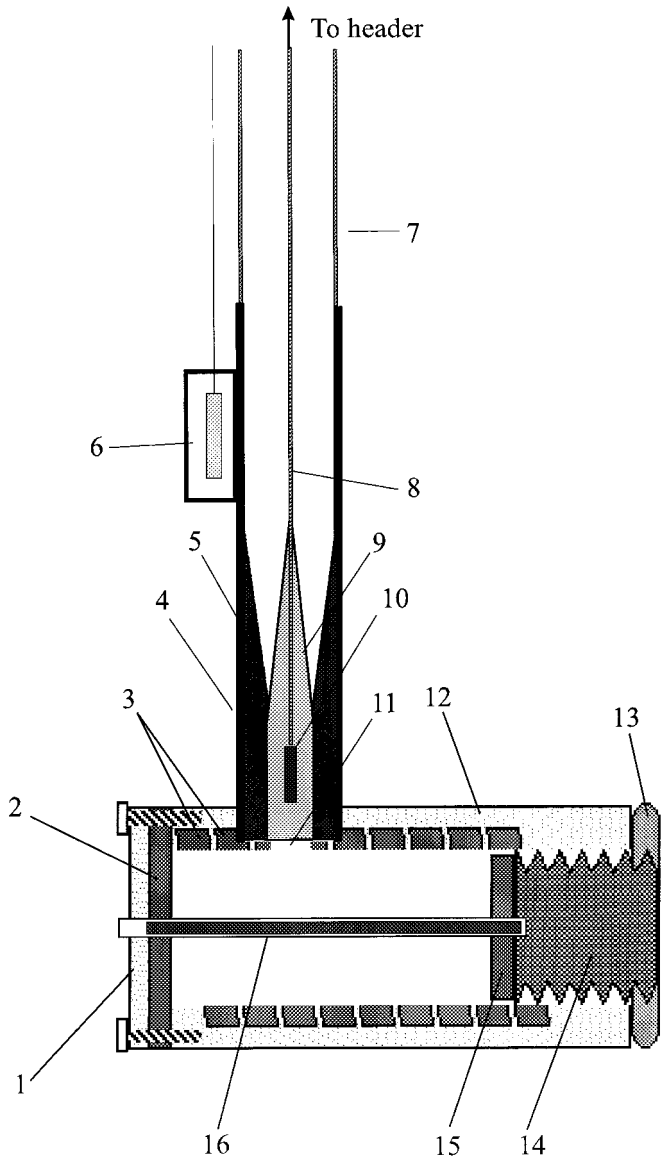

FIG. 3. Lower end of probe with Gordon coupler and cross-section of the helical cavity: (1) epoxy end-cap, (2) brass end-wall attached to the epoxy end-cap, (3) brass helix forming the cavity, (4) brass waveguide with Gordon coupler, (5) brass tapered section, (6) carbon-glass temperature sensor inside brass shield, (7) stainless steel waveguide, (8) exterior stainless steel rod connecting fin to micrometer on header, (9) teflon wedge, (10) teflon fin protruding from waveguide, (11) coupling iris, (12) epoxy shell holding the helix, (13) C-8 plunger locking disc, (14) threaded epoxy plunger, (15) brass wall on plunger, (16) sample tube.

area, and >95% at 12.5 kHz. The solid metal causes some attenuation of the modulation field but significantly improves the stability of the walls.

A major problem with this cavity design is the noise caused by the interaction of the modulation and static magnetic fields with the metallic parts of the cavity. In the $\mathbf{B_1} \parallel \mathbf{B}$ orientation the interaction between the eddy currents, induced on the end wall and plunger, and the static field can give rise to Lorentz forces which cause wall vibrations and noise in the EPR signal. This problem is absent in the $\mathbf{B_1} \perp \mathbf{B}$ configuration, and consequently, we have lower spurious modulation signals. The noise problem is minimized in the parallel mode by fastening the end wall and plunger firmly onto the cavity. The end wall is screwed tightly onto threaded brass posts cast inside the epoxy shell of the cavity and the plunger is locked against the epoxy body of the cavity via a plastic locking disc (no. 13, Fig. 3). Our ability to tune the frequency of the cavity at low temperatures is therefore eliminated, so tuning is made at room temperature and appropriately adjusted to account for the frequency shift of the cavity when cold.

The brass cavity was electroplated with gold (*13*). The stock plating solutions of $KAu(CN)_2$ (12 g/L), KCN (20 g/L) (Aldrich Chemical Company), K_2HPO_4 (20 g/L) (Fisher), and K_2CO_3 (20 g/L) (Aldrich) were treated with Chelex 100 resin (Bio-Rad Laboratories) to remove metal impurities. Plating at a temperature of 50–60°C and current density of 10^{-3} A/cm^2 deposited a layer of 4–6 μm of gold on the inner wall of the helix, which is large compared to the skin depth at 34 GHz (400 nm), and small compared to that at 100 kHz (200 μm) at liquid helium temperatures.

Following the method described by Dalal *et al.* (*14*), the unloaded Q of the cavity with brass helix and wall/plunger was found to be 1200 at room temperature. This Q is lower than that of most other cavities due to the cylindrical wall coupling, which decreases the theoretical Q by a factor of approximately three compared to the conventional end-wall coupling (*12*). The gold-plated unloaded Q is 1400 and when loaded with a sample tube of 2.4 mm o.d. and 2 mm i.d. (Wilmad Glass), the Q drops to 1200. Smaller diameter tubes (2 mm o.d./1 mm i.d.) have much smaller sample volume and consequently gave weaker signals, whereas larger tubes (3 mm o.d./2.5 mm i.d.) shift the cavity frequency too far and required a plunger position overlapping with the coupling iris, causing unwanted reflections of the incident microwave radiation.

Microwave Probe

The EPR probe consists of a coin silver E-bend (Millitech Corp., South Deerfield, MA) mounted inside the header assembly of our cryostat and connected to a straight section of WR-28 brass waveguide via a choke flange. The entire header assembly is vacuum tight to allow pumping on the liquid helium bath to lower the sample temperature to ~1.5 K. The brass waveguide is attached, via a choke flange, to a straight 4 in. long piece of stainless waveguide to reduce thermal conduction. The stainless waveguide is soldered onto a brass waveguide housing a Gordon coupler, which allows variable coupling of the cavity to the waveguide (*15*). The end of this piece extends into the epoxy body of the cavity, with the teflon wedge directly above the coupling iris on the helix (Fig. 3).

The cavity is mounted on the waveguide with a rectangular piece of fiberglass cradle. One side of the cradle is machined to a diameter matching the o.d. of the cavity. The cradle is screwed onto four threaded brass posts attached to a flange on the waveguide, thus clamping the cavity against the waveguide.

Metallic tapers in the Gordon coupler reduce the cross-sectional dimensions of the WR-28 waveguide to 0.149 × 0.140 in. to bring the waveguide below the cutoff frequency (ν_c = 21.10 GHz) for propagation of the microwave radiation. A teflon wedge (dimensions: 0.149 × 0.140 × 0.443 in. tapered to an apex angle of 5°) is inserted into the taper to bring the guide wavelength above cutoff and thus allow propagation of the microwaves into the cavity. To avoid having a control rod inside the waveguide, and corresponding microwave reflection difficulties (*16*), we constructed the teflon wedge with a "fin" protruding out of the waveguide through a nonradiative slot along the middle of the broad face of the waveguide. The teflon wedge is controlled from the header through a long stainless steel tubing (0.010 in. wall) which is attached to a micrometer.

Modulation

Field modulation is provided by a pair of coils, 2.25 in. apart in a near-Helmholtz arrangement mounted outside the cryostat tail. Each coil has 160 turns of Litz wire (NELB66/38SPSN New England Electric Wire Corp., Lisbon, NH) with an average diameter of 1 in. and a thickness of $\frac{1}{2}$ in. The coils present an r.f. impedance at 100 kHz of 12 Ω and are powered by a broadband ENI 1040L power amplifier. The matching to the 50 Ω impedance of the power amplifier is achieved by the use of a parallel/series capacitor circuit for optimum delivery of r.f. power to the coils (*17*). We chose to mount the coils outside the cryostat to avoid heating and boiling of the liquid helium and subsequent signal noise, which occurs when the coils are immersed in the bath. A near-Helmholtz arrangement is used in order to reduce the diameter of the coils to about the same diameter as the cavity to prevent substantial heating of metallic parts of the cryostat tail and the probe and the two temperature sensors around the cavity. Mapping of the modulation field intensity indicated that the value of $\mathbf{B}_{mod}$ dropped by ≤3% between the center of the cavity and the walls and by ≤1% between the center and the side wall. Another pair of modulation coils with similar specifications were constructed to operate at 12.5 kHz. The $\mathbf{B}_{mod}$ produced at the sample at liquid helium temperatures was measured both by direct measurement of the voltage from a calibrated pickup coil and from the broadening of one of the sharp hyperfine lines of Mn^{2+} (linewidth 1 G) present as impurity in a powder sample of CaO.

To afford greater $\mathbf{B}_{mod}$ at the sample and to maximize the cooling efficiency of the radiation shield, we designed a fiberglass cryostat tail with a slotted radiation shield. The shield is an aluminum tube with thin strips cut along the tube axis from above the cavity region to the end of the tube. Care was taken to eliminate any conducting loops in planes perpendicular to $\mathbf{B}_{mod}$, which may occur in the radiation shield or the cavity.

Anaerobic Exchange of Oxygen-Sensitive Samples

Many of the samples under study are oxygen sensitive in solution and must be loaded frozen. Due to the orientation of our cavity, it is impossible to load samples while the EPR probe is inside the cryostat; the probe must be removed from the cryostat and sample exchange must occur outside the cryostat. To achieve this without thawing the samples, we designed a telescoping acrylic dome which is attached directly above the cryostat. In its lowered position, the bottom part of the dome rests on an 8-in. aluminum plate on the cryostat. A hole with a diameter of 1.5 in. is drilled close to the edge of the acrylic dome for sample loading. This allows us to withdraw the probe from the cryostat in a dry helium gas atmosphere, remove the sample while the cavity is still cold, and load a new frozen sample. The probe is then lowered into the cryostat and sample exchange has been achieved without thawing the sample. The dome is then raised to allow adjustment of the controls on top of the header. The entire sample change procedure, including probe cool down to liquid helium temperature, takes approximately 20 min.

Additional Spectrometer Components

All of our measurements were carried out at liquid helium temperatures in an immersion-type cryostat with a fiberglass tail section (CRYO Industries of America, Atkinson, NH). The temperature was controlled by a temperature controller (Model 340, LakeShore, Westfield, OH). We used two calibrated temperature sensors: a GaAlAs diode (TG-120CU) in the liquid helium vaporizer and a carbon-glass resistor (CGR-1-1000, LakeShore) on the EPR probe (no. 6, Fig. 3). Our probe was connected to a Bruker microwave bridge (ER051QG) controlled by an ER200D console. The microwave frequency was measured by a microwave frequency counter (HP 5352B), and an NMR gaussmeter (Bruker ER035) was used to calibrate the magnetic field strength. The data were acquired and analyzed with software developed in our lab. The sensitivity of the new probe was tested on various samples of which we report data from Fe^{2+} in zinc fluorosilicate and hemerythrin.

RESULTS

Single crystals of zinc fluorosilicate doped with low concentrations of iron have proven to be useful as a quantitation standard for integer-spin systems (*1*). Crystals were grown from solutions of fluorosilicic acid (H_2SiF_6) (Aldrich Chemical Co.) with saturating amounts of zinc or iron metals (J. T. Baker, Inc.) in the appropriate ratio. Crystals were mounted onto quartz flats so as to align the crystalline axis of symmetry (*c* axis) parallel to the axis of symmetry of the cavity, and thus parallel to $\mathbf{B}_1$. The crystals were covered with a thin layer of silicone grease to prevent deterioration and then frozen in liquid nitrogen. The Fe/Zn ratio was determined by plasma emission spectroscopy to be 0.0029.

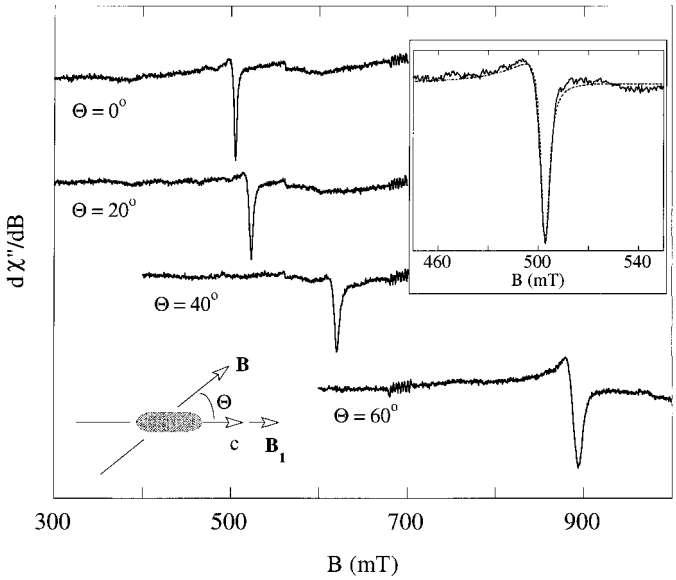

FIG. 4. Angular variation of the Q-band spectra of Fe^{2+} in zinc fluorosilicate. The magnetic field **B** is rotated through angles θ from the *c* axis of the crystal in a plane perpendicular to the axis of symmetry of the probe. The inset shows a blow-up of the line at $\theta = 0°$ (solid line) with simulation (dotted line). Instrumental parameters: temperature, 10 K; microwave, 34.043 GHz at 0.1 mW; modulation, 12.5 kHz at 4.9 G_{pp}. Simulation parameters: $D = 14.3\ cm^{-1}$, $E = 0$, $\sigma_E = 0.024\ cm^{-1}$, $g_z = 2.415$. Sample: crystal; mass, 10 mg; Fe/Zn ratio, 0.0029.

The quintet energy levels of the high-spin ferrous ion ($S = 2$) are parameterized in terms of the spin Hamiltonian

$$\mathcal{H} = D(S_z^2 - 2) + E(S_x^2 - S_y^2) + \beta \mathbf{B} \cdot \mathbf{g} \cdot \mathbf{S}, \qquad [2]$$

where the axial zero-field splitting is $D = 14.3\ cm^{-1}$ (*18*) and the rhombic splitting is $E \approx 0\ cm^{-1}$ (*19*).

The EPR signals at 35 GHz are shown in Fig. 4 for rotations of **B** relative to the crystal for $0 < \theta < 60°$. The signal originates from the first excited doublet of the spin quintet. This doublet is split in zero-field by $\Delta_1 = 2E$, with eigenfunctions $|\pm 1'\rangle = |m_s = +1\rangle \pm |m_s = -1\rangle$ as shown in Fig. 1. The sharp asymmetric line has a turning point at $g = h\nu/\beta B = 4.85$. The angular variation is in agreement with the prediction of the resonance condition, Eq. [1], taking into account a small misalignment in the plane of rotation of the crystal with respect to **B.** For $\theta > 60°$ the line quickly moves

to resonance positions greater than our maximum field strength.

The integrated intensities (after correcting the normalization to account for the magnetic field sweep (*20*)) of the signals of Fig. 4 are independent of the direction of **B.** In contrast, odd electron centers have a strong dependence of intensity with respect to the direction of **B.** This is easily explained with consideration of the intensity of an EPR line for a transition between the states $|m\rangle$ and $|n\rangle$, which is proportional to $|\langle m|\mathbf{B_1} \cdot \mathbf{g} \cdot \mathbf{S}|n\rangle|^2$ (*3, 10*). For odd-electron centers, **S** is quantized along the direction of the magnetic field (for anisotropic *g* tensors, the same is true but the quantization axis is then $\mathbf{g} \cdot \mathbf{S}$ (*21*)). The product $\mathbf{B_1} \cdot \mathbf{g} \cdot \mathbf{S}$, and thus the intensity, changes as **B** is rotated, since **S** tracks with **B.** For even-electron centers, **S** is fixed with respect to the ligand field of the metal center and does not follow **B** for low magnetic fields, thus $\mathbf{B_1} \cdot \mathbf{g} \cdot \mathbf{S}$ is a constant if only **B** is rotated, as we observe in Fig. 4. If the crystal is rotated instead, then **S** will change relative to $\mathbf{B_1}$ and the intensity will now vary (*19*).

Simulations of spectra are essential for quantitative analysis, because the simulations allow determination of the intrinsic intensity of the spectrum for a given number of moles of metal ions. The standard determination of spin concentration by double integration of the spectra is not appropriate due to the large change in the transition probability over the full signal. Simulations of the spectra for $\theta = 0°$ are shown in the inset of Fig. 4. The simulations assume that the dominant source of broadening is from a distribution in the zero-field splitting of the metal (*1*). Small variations in the ligand field strength for molecules in the crystal result in a spread of the *D* and *E* values. The EPR signal linewidth of the Fe^{2+} fluorosilicate is thus broadened due to the dependence $\Delta_1 = 2E$. The signals are simulated with a Lorentzian distribution in the *E* value centered at 0 cm^{-1} with a standard deviation of 0.024 cm^{-1}.

Our main interest in developing the probe presented here is for the study of metalloproteins with even electron systems. Hemerythrin (Hr) is the oxygen transport protein of marine invertebrates (*22*) containing one diiron cluster per monomeric subunit of protein. The protein has been relatively well characterized electronically and structurally (*22, 23*). The azide adduct of deoxyHr contains two ferrous sites bridged by a water molecule. The two high-spin $S = 2$ iron sites are ferromagnetically exchange coupled with $J = -3.4\ cm^{-1}$ (*24*).

Frozen solution EPR spectra of deoxyHr N_3 are shown in Fig. 5 at 35 GHz with $\mathbf{B_1} \parallel \mathbf{B}$ and $\mathbf{B_1} \perp \mathbf{B}$. To our knowledge, these are the first EPR spectra of a metalloprotein at 35 GHz with $\mathbf{B_1} \parallel \mathbf{B}$. The simulations overlaid on the data (dashed lines) use the parameters originally published in our previous work (*24*). Using the Fe/Zn fluorosilicate sample as the concentration standard, the simulations of the fluorosilicate (Fig. 4) and Hr data allow determination of the concentration of the Hr sample. Comparison of ratios of data and simulated intensities gave a Hr concentration of 7.8 mM. This value is 30% higher than the known protein concentration of 6 mM. The calculation takes into account the different filling factors of the fluorosilicate crystal (10 mg) and frozen solution Hr tube sample (35 μL in quartz tube, i.d. = 2 mm). We ignored the correction for $\mathbf{B_1}$ magnification due to the differing amounts of quartz at the sample, which may be a significant contribution to the difference between the two values. In future work, we intend to improve the quantitation standard to better mimic the protein in sample tubes. Nevertheless, the agreement is comparable to quantitation of general protein samples on commercial instrumentation and sufficiently accurate to pursue protein studies.

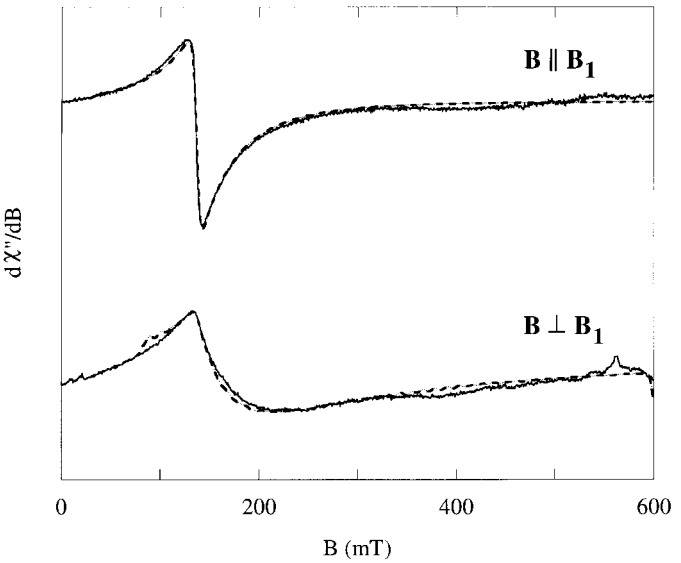

FIG. 5. Q-band spectra of deoxyHr azide (solid lines) with simulations (dotted lines). Instrumental parameters: temperature, 7K; microwave, 34.071 GHz at 1 mW; modulation, 12.5 kHz at 3.6 G_{pp}; gain, 10^4. Simulation parameters: $D = 2.92\ cm^{-1}$, $E = 0.45\ cm^{-1}$, $\sigma_E = 0.21\ cm^{-1}$, $g_y = 2.23$. Sample: frozen solution; MES pH 6.0; protein concentration, 6 mM.

CONCLUSION

We have successfully constructed a Q-band probe with sufficient sensitivity to allow observation of signals from even electron metalloproteins. Spectra from these so-called "EPR-silent" proteins can now be observed with at least two different microwave frequencies with $\mathbf{B_1}$ parallel and perpendicular to **B.** We have demonstrated that the signals from the new instrument can be quantitatively analyzed to determine protein concentrations, which will be important for future studies.

ACKNOWLEDGMENTS

We thank Dr. N. D. Chasteen and Dr. R. A. Isaacson for useful discussions early on in the project. We also acknowledge the use of some microwave and cryogenic equipment kindly provided by professors N. S. VanderVen and S. A. Friedberg of the Carnegie Mellon Physics Department. This work was supported by NIH Grant GM49970 and the Searle Scholars Program.

REFERENCES

1. M. P. Hendrich and P. G. Debrunner, *Biophys. J.* **56,** 489 (1989).
2. M. P. Hendrich and P. G. Debrunner, *in* "Foundations of Modern EPR" (G. R. Eaton, S. S. Eaton, and K. M. Salikhov, Eds.), p. 530, World Scientific, Singapore (1998); W. R. Hagen, *Biochim. Biophys. Acta* **708,** 82 (1982); S. L. Dexheimer and M. P. Klein, *J. Am. Chem. Soc.* **114,** 2821 (1992); T. Yamauchi, H. Mino, T. Matsukawa, A. Kawamori, and T. Ono, *Biochemistry* **36,** 7520 (1997); K. A. Campbell, J. M. Peloquin, D. P. Pham, R. J. Debus, and R. D. Britt, *J. Am. Chem. Soc.* **120**(2), 447 (1998).
3. A. Abragam and B. Bleaney, "Electron Paramagnetic Resonance of Transition Ions," Section 3.14, Dover, New York (1985).
4. J. A. J. M. Disselhorst, H. Van der Meer, O. G. Poluektov, and J. Schmidt, *J. Magn. Reson. A* **115,** 183 (1995).
5. J. W. A. Coremans, O. G. Poluektov, E. J. J. Groenen, G. W. Canters, H. Nar, and A. Messerschmidt, *J. Am. Chem. Soc.* **116,** 3097 (1994); *J. Am. Chem. Soc.* **118,** 12141 (1996).
6. A. L. Barra, D. Gatteschi, R. Sessoli, G. L. Abbati, A. Cornia, A. C. Fabretti, and M. G. Uytterhoeven, *Angew. Chem. Int. Ed. Engl.* **36,** 2329 (1997); L. R. Becerra, G. J. Gerfen, B. F. Bellew, J. A. Bryant, D. A. Hall, S. J. Inati, R. T. Weber, S. Un, T. F. Prisner, A. E. McDermott, K. W. Fishbein, K. E. Kreischer, R. J. Temkin, D. J. Singel, and R. G. Griffin, *J. Magn. Reson. A* **117,** 28 (1995); J. Telser, L. A. Pardi, J. Krzystek, and L.-C. Brunel, *Inorg. Chem.* to appear.
7. A. Sienkiewicz, B. G. Smith, A. Venelov, and C. P. Scholes, *Rev. Sci. Instrum.* **67,** 2134 (1996); K. R. Mercer and W. A. Bernhard, *J. Magn. Reson.* **74,** 66 (1987).
8. W. Wang and N. D. Chasteen, *J. Magn. Reson. A* **116,** 237–243 (1995).
9. C. P. Poole, *in* "Electron Spin Resonance," (Second Edition, Chap. 5, Wiley, New York (1983).
10. J. A. Weil, J. R. Bolton, and J. E. Wertz, *in* "Electron Paramagnetic Resonance," pp. 480, 508, Wiley–Interscience, New York (1994).
11. H. E. M. Barlow, H. G. Effemey, and P. H. Hargrave, *Proc. Inst. Elec. Engrs.* (London) *B* **107,** 66 (1960); A. J. Estin, *Rev. Sci. Instr.* **33,** 369 (1962).
12. I. G. Wilson, C. W. Schramm, and J. P. Kinzer, *Bell Syst. Tech. J.* **25,** 408 (1952).
13. F. A. Lowenheim (Ed.), "Modern Electroplating," Wiley–Interscience, New York (1974).
14. D. P. Dalal, S. S. Eaton, and G. R. Eaton, *J. Magn. Reson.* **44,** 415 (1981).
15. J. P. Gordon, *Rev. Sci. Instr.* **32,** 658 (1961).
16. R. A. Isaacson, *Rev. Sci. Instr.* **47,** 973 (1976).
17. H. L. Krauss, C. W. Bostian, and F. H. Raab, "Solid State Radio Engineering," Wiley, New York (1980).
18. F. Varret, *J. Phys. Chem. Solids* **37,** 257 (1976).
19. M. P. Hendrich and P. G. Debrunner, *J. Magn. Reson.* **78,** 133 (1988).
20. J. R. Pilbrow, *in* "Transition Ion Electron Paramagnetic Resonance," Section 1.6, Clarendon Press, Oxford (1990).
21. G. E. Pake and T. L. Estle, "The Physical Principles of Electron Paramagnetic Resonance," Benjamin, Elmsford, NY (1973).
22. I. M. Klotz and D. M. Kurtz, Jr., *Acc. Chem. Res.* **17,** 16 (1984); P. C. Wilkins and R. G. Wilkins, *Coord. Chem. Rev.* **79,** 195 (1987); K. Zhang, E. A. Stern, F. Ellis, J. Sanders-Loehr, and A. K. Shiemke, *Biochemistry* **27,** 7470 (1988).
23. R. C. Reem and E. I. Solomon, *J. Am. Chem. Soc.* **109,** 1216 (1987).
24. M. P. Hendrich, L.L. Pearce, L. Que, N. D. Chasteen, and E. P. Day, *J. Am. Chem. Soc.* **113,** 3039 (1991).